Materials and Design 95 (2016) 623–631

Contents lists available at ScienceDirect

Materials and Design

journal homepage: www.elsevier.com/locate/matdes

The significance of specimen displacement definition on the mechanical properties derived from Small Punch Test

M.F. Moreno [a,b], G. Bertolino [a,b,d,*], A. Yawny [a,b,c,d]

[a] División Física de Metales, Centro Atómico Bariloche, Av. Bustillo 9500, 8400 S. C. de Bariloche, Argentina
[b] CONICET, Argentina
[c] CNEA, Argentina
[d] Instituto Balseiro, CNEA-UNCuyo, Argentina

ARTICLE INFO

Article history:
Received 7 January 2016
Received in revised form 28 January 2016
Accepted 30 January 2016
Available online 1 February 2016

Keywords:
Small punch testing
Reduced size specimen
Mechanical characterization
Finite element method

ABSTRACT

The different displacements definitions used for describing the Small Punch Tests (SPT) material response were thoroughly reviewed. For that purpose, an instrumented experimental setup allowing determining the specimens top or bottom displacement together with the machine cross head displacement was designed. The effects of the machine and load train compliances on the respective displacements values were carefully evaluated. The significance of the different displacements definitions was demonstrated by proposing two alternative procedures for assessing the specimen thickness evolution and by revising the definition of the load associated with the determination of the material yield stress from SPT. To facilitate the systematic study of the influence of the different parameters that might be affecting the test, a finite element (FEM) analysis tool was developed. The results obtained from FEM simulations show that even using a constitutive model that does not include damage initiation it is possible to adequately reproduce the SPT load vs. displacement response curve to near maximum load and also the diametral profiles of the deformed specimens. The FEM analysis indicate the arbitrary character of the different proposals for determination of the load for yield stress estimation with them corresponding to different degrees of plastic deformation of the specimen.

1. Introduction

The interest on miniaturized specimen techniques for the characterization of the mechanical behavior of materials was strongly motivated by the different programs associated with the development of fusion reactor technology in the early eighties [1]. The importance of such developments is obvious in the case of the nuclear industry where neutron irradiation space is limited and irradiation costs increase with specimen volume. In addition, the limited space available in materials testing reactors (MTR), the presence of neutron fluence gradients in large specimens, the concern about gamma heating and dose to personnel in post-irradiation testing have all been motivations for reducing specimen size [2–5].

In their seminal work, Manahan et al. [2] developed a miniaturized disk bend test for the determination of the mechanical properties of materials after irradiation. Simply supported 3 mm in diameter, 0.25 mm thick, TEM sized disk specimens were deformed through a 2.46 mm in diameter bore using a 1 mm in diameter hemispherical punch. Finite element modeling (FEM) was employed in that case to simulate the deformation of the disk. These authors also intended to apply FEM in an inverse procedure which would allow deriving strength and ductility properties from the load vs. displacement response of the disk center. Success, however, was rather limited.

Considering the substantial advantages related with the application of small scale technologies, it has also been intended to extend its use to non-nuclear industries like fossil fuel energy production plants. The main driving force for reducing specimen size in this case resides in the scarcity of the material to be characterized (i.e., along the process of developing new materials), limitations of testing machines capacity or in the presence of microstructural gradients in thick sections which prevents the use of standard macroscopic specimens in situations where the properties of a particular microstructure wants to be assessed (e.g. heat affected zone, HAZ, in welded joints).

The small punch test SPT has been considered for the evaluation of a wide range of mechanical properties, including strength, ductility, fracture toughness, ductile–brittle transition temperature and high temperature behavior (creep) [6–13]. Most of the researches use a specimen clamped between two rigid dies, a configuration sometimes referred to as "bulge punch tests" for some authors, e.g. [5]. Due to its wide actual acceptance, in the context of the present work, SPT will be used to refer to ball punch testing of clamped specimens.

Four different deformation regimes were identified in a typical SPT P–δ (load vs. displacement) response. The consecutive stages are [8]: (I) elastic bending of the disk and microyielding under the punch, (II) plastic bending of the disk, with plasticity spreading, firstly through

* Corresponding author.
E-mail address: bertolin@cab.cnea.gov.ar (G. Bertolino).

http://dx.doi.org/10.1016/j.matdes.2016.01.148
0264-1275/

the thickness under the punch contact area and then radially outwards, (III) membrane stretching and, finally, (IV) local thinning and crack initiation. However, it is worthwhile to remark here that the precise definition of the boundaries between the different regimes is rather subjective.

On the other hand, a profuse number of semi-empirical relations derived from experimental information have been proposed in the literature that would allow extracting parameters such as yield stress, yield strength, uniform elongation or estimations of shifts in the ductile to brittle transition temperature from punch tests (e.g., see [10,14–19]). For example, the yield stress σ_Y could be estimated from a load P_Y associated with the transition between deformation regimes I and II while a ductile to brittle transition temperature (DBTT) from the temperature dependence of the fracture energy E^{SPT} calculated as the area under the load vs. punch displacement curve. These correlations however, have been shown to be sensitive to the characteristics of the particular material under study [20] and to the different experimental parameters associated with the technique like the specimen diameter and thickness, bore size, friction coefficient and clamping force between disk and dies, ball dimension, ball material properties and friction between ball and specimen, among others. Assessing the relative importance of the different parameters on the specimen response is mandatory for a correct application of the technique. With this purpose, Lucas, Okada and Kiritani [21], experimentally investigated the effects of ball and bore size and specimen thickness on the load vs. displacement response of different materials deformed in a bulge punch test configuration in what constituted the first parametric analysis of these miniature specimen procedures. Later, using finite element method (FEM), Sainte-Catherine and co-workers [22] performed a parametric study of the effect of thickness, clamping conditions and friction coefficient on the SPT response. The effects of yield stress, hardening behavior, specimen thickness and ball-specimen friction on the response of AISI 316L and F82H-mod tempered martensite steel to SPT tests on 3 mm in diameter disks were investigated by Campitelli et al. [23] using FEM modeling. Similarly, Peñuelas et al. [13] have performed extensive numerical simulations to obtain mechanical and damage properties of steels from the load–displacement curve obtained from SPT and considered the influence of friction coefficient and hardening behavior on the SPT response.

There is however an important factor whose influence is often ignored and this is the way in which the value of the displacement used for representing the P–δ response is determined. In spite of its significance, there are no systematic studies on this issue and only few authors have paid attention to the different possibilities for the displacement determination, i.e., disk top or bottom central point displacement, machine cross head displacement, etc., and to the effects of the machine and load train compliances on the respective values [23–28]. In the present work, a thorough analysis is performed with the aim of clarifying this matter. It includes the revision of the definition of the load P_Y associated with determination of the material yield stress σ_Y and of the evaluation of the fracture energy E^{SPT}, values which might depend on the displacement parameter adopted as representative of the specimen deformation. In addition, two alternative procedures for the assessment of the specimen thickness evolution along the test will be proposed.

Due to the higher complexity associated with SPT characterization and to facilitate the systematic study of the influence of the different parameters that might be affecting the test, FEM was used here to simulate the experimental response. The material constitutive law was incorporated using a von Mises definition of effective stress vs. effective strain using the behavior determined from uniaxial tests. The high strain levels associated with SPT in comparison with uniaxial tensile testing requires extrapolation of the stress–strain values obtained from uniaxial tests. The appropriateness of different extrapolation criteria and the need of introducing a damage-law are discussed based on the comparison between experimental and simulated results. In that way, the modeling tool was first validated and then applied to the analysis of the physical significance of specific features associated with the SPT mechanical response.

2. Experimental details

2.1. SPT equipment and testing

The SPT mechanical characterization was performed on disks specimens with a diameter $D = 10$ mm using the specimen holder schematically illustrated in Fig. 1. It consists in demountable upper and lower dies, a puncher, a 2.5 mm in diameter Si_3Ni_4 ceramic ball and different transducers for displacement determination. The dies were fabricated in 28 HRC Cr–Mo steel. The SPT disk specimen is centered in the lower die receiving hole, also 10 mm in diameter. A clamping force is applied by tightening four metric Allen M4 bolts between the upper and the lower die. The inferior bore of the lower die has a diameter $d = 4$ mm with a beveled edge transition with a radius $r = 0.5$ mm.

The specimen holder was disposed in the frame of an electromechanical testing machine Instron 5567, ±30 kN maximum load capacity, using an additional support base disposed in the manner illustrated in Fig. 2. The displacement value determined from the optical encoder of the testing machine will be referred to as the nominal displacement δ_N. In the present work, all SPT tests were performed under constant displacement rate conditions (CDR in what follows) using a nominal displacement rate of 0.1 mm/min. The load response was followed by a drop-through Instron Series 2525 ± 1 kN, alternatively ±5 kN, full scale load cell disposed in series with the plunger.

The displacements δ_{TOP} and δ_{BOT} indicated in Fig. 1 correspond to the relative displacement of the center of the upper face of the disk with respect to the die and the relative displacement of the center of the disk bottom face with respect to the die, respectively. In the initial stages of deformation, δ_{TOP} includes the displacements associated with the elastic and plastic indentation of the ceramic ball into the specimen. In later stages, the difference between both values is mainly related with the specimen thickness evolution during deformation. Of them, only δ_{BOT} might be directly evaluated from the test. In the present study, the deflection δ_{BOT} was determined using an inductive displacement transducer (HBM W1T3, ±1 mm) housed in the support base (Fig. 2) and a HBM Spider 8 signal conditioner and amplifier. The determination of the displacement δ_{TOP} is often approached by different authors by measuring a displacement indicated in the present work as δ_{EXT}. This is done

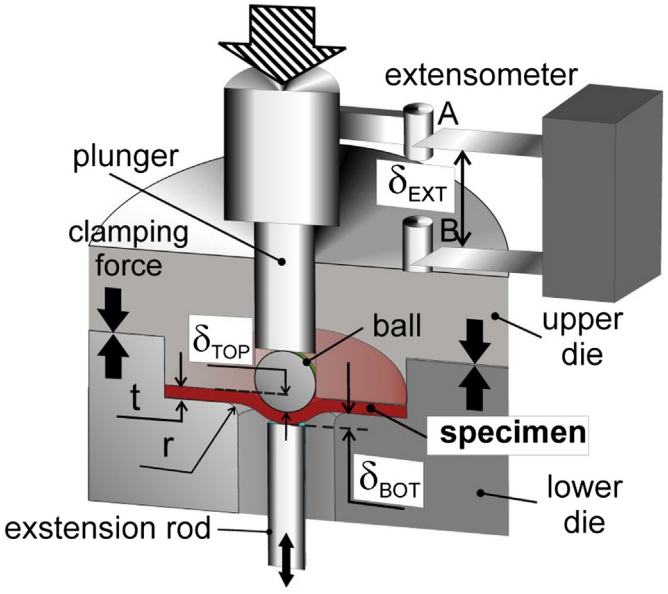

Fig. 1. Schematic illustration of the SPT specimen holder indicating main components and different displacements considered.

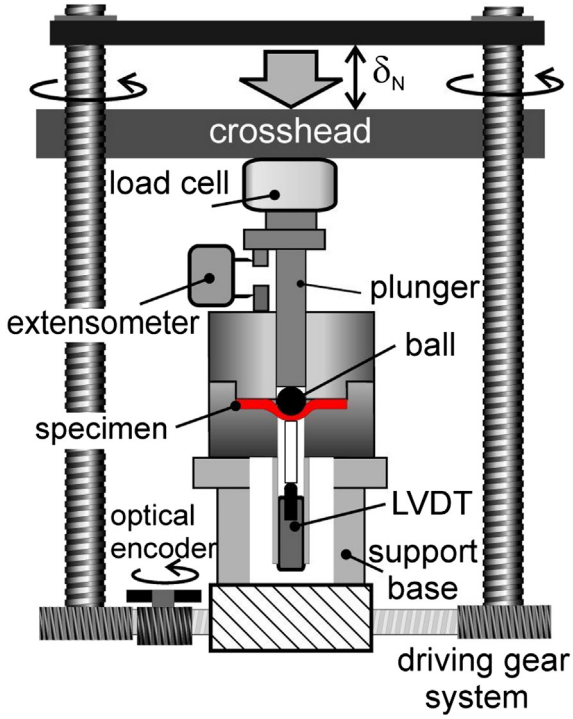

Fig. 2. Schematic of the specimen holder disposed in the frame of the testing machine Instron 5567. The nominal displacement δ_N is indicated.

by affixing an extensometer in the way illustrated in Figs. 1 and 2 [27–29] or using a linear variable displacement transducer LVDT attached to the crosshead of the testing machine [30]. However, it is important to remark that the precise assessment of δ_{TOP} from the experimentally determined δ_{EXT} can only be made by an appropriate experimental determination of the effective stiffness of the plunger length involved (vertical distance between point A and top of the ball in Fig. 1) and the ceramic ball itself. The SPT device here designed allows measuring the displacement δ_{EXT} of the puncher with respect to the die using an extensometer (MTS 632.12C-20, 25 mm gage length, 12.5 mm maximum opening aperture).

The nominal displacement δ_N might also be used for assessing the displacement δ_{TOP}. However, this requires an appropriate calibration of the effective stiffness of the whole loading system including machine frame, specific load cell employed, plunger, ceramic ball and support base.

The significance of the different displacement definitions and the relationships between them will be analyzed in further detail in following sections.

Before that, it has to me mentioned that the consistency of the results obtained with the SPT experimental setup here designed was checked by verifying the reproducibility of the P–δ curves corresponding to several tests performed with the same material under the same conditions.

2.2. Materials and SPT specimen preparation

The material adopted for the present study was AISI 304L stainless steel circular bar with a 25% area reduction by cold work. For preparing the SPT specimens, the original rod diameter was reduced from 12 mm to 10 mm by turning and then 1 mm thick slices were cut from these rods using a low speed metallographic saw. The slices were then grounded and mechanically polished using 1200 grit paper down to the final thickness with a tolerance of ± 5 μm. Great care was put on obtaining parallel surfaces by using a special disk holder. Final lapping of both circular faces was performed using colloidal alumina suspensions from 5 μm to 0.05 μm. Thickness was determined with a 1 μm resolution digital micrometer. Disk specimens with thicknesses $t = 400$, 500 and 600 μm were prepared.

To obtain the profile along diametral cross-sections after testing, some deformed SPT specimens were included in plastic resin and then they were cut and polished following standard procedures.

2.3. Uniaxial tensile tests

In order to determine the uniaxial tensile properties of the materials considered, complementary uniaxial tensile tests were conducted at room temperature using cylindrical standard specimens and initial nominal strain rates of $1.2 \times 10–3\ s^{-1}$.

3. Numerical simulations

The deformation process associated with SPT was simulated using the Finite Element Method (FEM) working with the open code Cast3m (www-cast3m.cea.fr). An axisymmetric finite element model of the SPT arrangement with four nodes quadrilateral elements (Fig. 3) was used in order to simulate the entire SP test. The upper and lower steel dies have been modeled as linear-elastic bodies with Young Modulus $E = 210$ GPa and Poisson ratio $\nu = 0.3$. The ceramic puncher was also modeled as a linear elastic body assuming $E = 300$ GPa and $\nu = 0.27$. Effective stress–strain constitutive equation corresponding to AISI 304L was obtained by fitting the experimental true stress–strain uniaxial curve in the region of uniform deformation (before necking). As the local effective plastic strain of a SPT specimen can reach levels far exceeding the maximum strain accessible in the uniaxial test, it was necessary to extrapolate the tensile curves beyond necking. A von Mises definition for effective stress and strain was adopted with this purpose. In that way, uniaxial stress–strain data can be directly converted to effective stress–strain values. Different extrapolations criteria were considered in the present work and their impact on the simulated response will be discussed. Neither damage nor failure was taken into account in the FEM simulations. The appropriateness of this assumption will be discussed elsewhere under the light of the obtained experimental results.

Unilateral contact and friction between the specimen and upper and lower dies and also between the specimen and the ceramic puncher were assumed. Coulomb's friction model was adopted, i.e., the relative tangential slide between two contacting surfaces results in a load of value $\mu \cdot \sigma_N$ in the contact plane along the displacement direction. Here μ stands for the friction coefficient and σ_N for the stress normal to the contact plane. In order study the sensitivity of the P–δ response with the value of the friction coefficient, simulations with μ values in

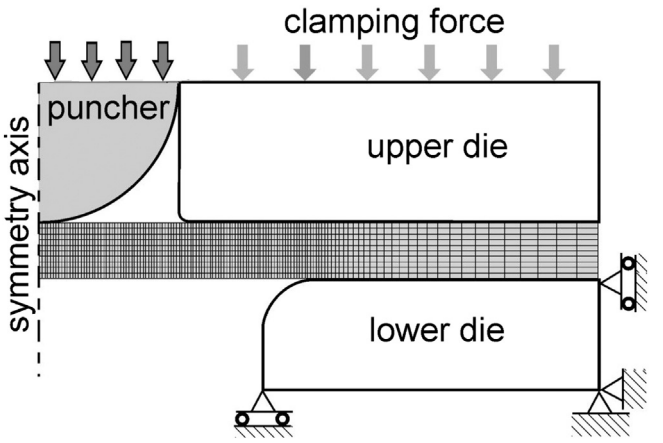

Fig. 3. Axisymmetric finite element model configuration employed for the FEM simulations performed with the open code Cast3m.

the range 0.1–0.9 have been performed. Results show that μ affects the curve only near maximum load, in line with the results of Peñuelas et al. [13]. As the tests conducted in the present study were made under unlubricated conditions, a value of $\mu = 0.5$ representing typical conditions for steel–Si_3Ni_4 contact was considered [31]. Taking into account the magnitude of the displacements involved in SPT, it was necessary to consider a large displacements situation for the simulations.

Mesh convergence analysis was made by recreating the mesh with a denser element distribution, reanalyzing and comparing the obtained P–δ curves to that of previous meshes until satisfactory stable results are obtained.

The simulations performed were intended to describe the load P developed as a consequence of the displacement imposed on the center of the spherical ceramic puncher. Additionally, the stress, strain and displacement fields along the disk have been obtained for posterior analysis. Fig. 3 illustrates the meshing and the boundary conditions assumed for the simulations.

4. Results and discussion

4.1. Tensile uniaxial behavior and extrapolation beyond necking

The true stress–true strain (σ–ε) response obtained from tensile test is shown in Fig. 4. The experimental data included in the figure correspond to the uniform deformation region, i.e., before necking. The conventional basic mechanical properties derived from these tests are summarized in Table 1.

As mentioned before, the maximum effective strains that can be reached in SPT greatly exceed the maximum uniform strain ε_U accessible in a uniaxial tensile test. Therefore, to have the effective stress vs. strain behavior at effective strains above necking for FEM simulations, linear and parabolic extrapolations of the uniform strain uniaxial data have been considered in the present work. In the first case, the σ–ε behavior has been linearly extrapolated from the point of maximum uniform deformation (arrow A in Fig. 4) considering the local slope of the curve at that point. The second is a two segments criterion. Firstly a parabolic fit of the experimental data corresponding to the uniform plastic deformation range was performed. The resulting function was considered to represent the material behavior in the strain range between the maximum uniform deformation (arrow A) and the maximum of the fitting parabola (arrow B in Fig. 4). From this last point on, a perfect plastic behavior was assumed.

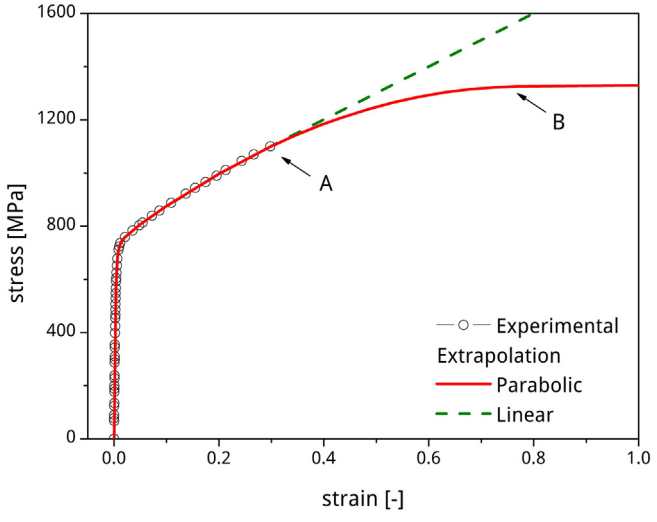

Fig. 4. Uniaxial true stress–true strain behavior of AISI 304L (25% area reduction by cold work) determined from tensile test and von Mises effective stress–effective strain curves obtained using linear and parabolic extrapolation criteria above necking (see text for details).

Table 1
Conventional basic tensile properties for the AISI 304L derived from the uniaxial tensile test shown in Fig. 4. E: Young's modulus; σ_{YS}: yield strength (0.2% off-set intersection method); σ_{TS}: tensile strength (nominal); ε_U: maximum uniform strain (true strain at instability).

E [GPa]	σ_{YS} [MPa]	σ_{TS} [MPa]	ε_U [–]
210	652	820	0.26

4.2. SPT: experimental results

4.2.1. Influence of displacement definition on the overall P–δ response

Fig. 5 shows SPT experimental P–δ curves for a specimen with a thickness $t = 0.500$ mm. The curves corresponding to the three displacements δ_N, δ_{EXT} and δ_{BOT} that can be directly determined from the tests were included in the plot. It can be seen that at the same load level $\delta_N > \delta_{EXT} > \delta_{BOT}$. This is a consequence of the differences in the finite elastic stiffness of the loading chains involved in each case. In effect, of the three parameters considered, only δ_{BOT} represents an actual displacement value of the specimen, i.e., the one corresponding to the center of the bottom face relative to the dies. As described before, δ_N and δ_{EXT} include displacements associated with the deformation of extra parts besides the displacement of the center of the upper face. The comparison of the three curves represented in Fig. 5 indicates the importance of specifying the displacement used for representing the SPT P–δ response. The question is somehow analogous to the situation posed in a tensile test when the knowledge of the stress vs. strain behavior might be intended to be derived from data corresponding to machine crosshead instead from an extensometer attached to the specimen.

The analysis of the results presented in Fig. 5 indicates that, on the one hand, a direct comparison of SPT responses obtained from different authors, most of the times using different devices and testing machine frames, would only make sense if the displacement δ_{BOT} is determined in all cases. Analysis of the literature shows that many authors adopt instead δ_N or δ_{EXT} as representative parameters and the reason is the simplicity of their determination. On the other hand, the determination of slopes and inflection points that might be associated with material properties like elastic modulus or yield stress would be affected by the displacement parameter adopted. The same occurs for the energy E^{SPT} associated with the area under the P–δ curve which is used for the determination of the ductile to brittle transition temperature and also in the evaluation of the displacement associated with maximum load for ductility determination.

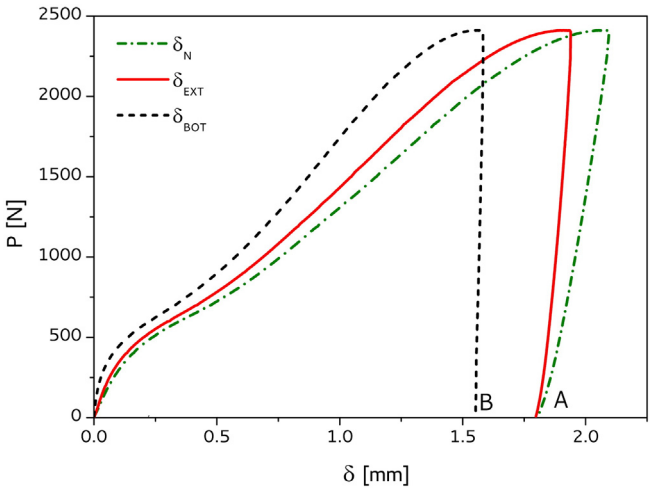

Fig. 5. Experimental P–δ curves for 0.500 mm thick specimen corresponding to the three displacements δ_N, δ_{EXT} and δ_{BOT} directly determined from the tests.

It can also be noticed from the curves presented in Fig. 5 that there is a difference among the slopes of the respective unloading paths with the unloading curves corresponding to displacements δ_N and δ_{EXT} converging to the same point in the null load condition (point denoted as A in Fig. 5). This fact constitutes a further confirmation that for other than zero loads the difference between the displacements δ_N and δ_{EXT} is due to the different finite elastic stiffness of the respective loading chains.

The displacement associated with the unloaded condition for δ_{BOT} (point denoted as B in Fig. 5) differs from the corresponding values for δ_N and δ_{EXT}. The displacement difference between points A and B represents the permanent thickness reduction δt_C^{pl} of the disk center corresponding to the load level reached before unloading. Here t_C represents the thickness of the disk center and the superscript *pl* denotes a permanent variation due to plastic deformation. This issue will be further analyzed in a next section.

4.2.2. Thickness evolution

As mentioned above, a possible way of following the evolution of the thickness of the center of the disk, t_C, along the test consists in performing several complete unloading–reloading cycles at progressively increasing maximum loads and assessing the difference between δ_{EXT} and δ_{BOT} at the respective null load. In this way, a discrete number of points describing the permanent (plastic) thickness reduction δt_C^{pl} as a function of a parameter representing the test progress (applied load or any of the displacements recorded) might be plotted. An alternative way of assessing the specimen thickness reduction along the test consists in continuously recording the displacements δ_{TOP} and δ_{BOT} and then subtracting δ_{TOP} from δ_{BOT}. By proceeding in that way, the continuous evolution of the total thickness reduction $\delta t_C = \delta t_C^{pl} + \delta t_C^{el}$ (plastic plus elastic) can be obtained as $\delta t_C = \delta_{BOT} - \delta_{TOP}$.

There are however some issues that have to be faced first. The displacement δ_{TOP} of the top face center of the disk respect to the die cannot be directly obtained from the experiments. Instead, its value can be derived from the displacements δ_N or δ_{EXT} through an appropriate calibration of the respective elastic compliances involved, referred to as C_N and C_{EXT}, respectively. For the experimental setup and testing machine configuration used in the present work these values were determined by testing a 3.25 mm thick tungsten carbide (WC) SPT disk specimen and recording the resulting load vs. displacement responses, i.e., P–δ_N^{WC} and P–δ_{EXT}^{WC}. One additional consideration is that the correct assessment of the compliance of the particular kinematic chain involved requires the subtraction of the displacement associated to the ceramic ball indentation into the WC specimen. Due to the difficulty of its experimental determination, this last contribution was computed by FEM assuming a linear elastic behavior for the WC disk. Finally, the displacement δ_{TOP} can be determined by subtracting from δ_{EXT} the displacement associated with the compliance calibration curves expressed as $P = C_{EXT} \cdot \delta_{EXT}$, alternatively $P = C_N \cdot \delta_N$.

Based on all previous considerations and in order to study the evolution of the thickness of the specimen center, a test up to maximum load was performed in a specimen with an initial thickness $t = 0.500$ mm. In addition, thirteen intermediate unloading-reloading cycles were performed. Fig. 6a illustrates the SPT response in terms of P–δ_{EXT} and P–δ_{BOT} curves. The P–δ_{TOP} curve shown in the figure was obtained from the experimentally determined P–δ_{EXT} by discounting the displacements of the compliance calibration curve $P = C_{EXT} \cdot \delta_{EXT}$ which corresponds to the curve shown at the left in Fig. 6a. For the sake of clarity, the intermediate unloading–reloading cycles were presented only in the P–δ_{EXT} curve. The first three unloading–reloading cycles were performed at the very beginning of the loading curve and therefore cannot be resolved in the figure.

The thickness variations δt_C^{pl} and δt_C were determined as described above. They are represented in Fig. 6b as a function of the displacement δ_{BOT}. The symbols (open circles) represent the permanent thickness variation δt_C^{pl} corresponding to the discrete number of intermediate unloading–reloading cycles while the continuous line shows the actual thickness variation δt_C. The slight difference between δt_C^{pl} and δt_C is the result of the additional thickness contraction due to the predominantly biaxial tensile stress existing in the center of the disk. The plot suggests the existence of a first stage with downwards curvature where the thickness reduction rate is high. This first region is followed by a displacement interval, δ_{BOT} between 0.200 and 0.450 mm, where the reduction rate exhibits a nearly constant value. Above 0.450 mm, a gradual increase of the thinning rate is observed until a displacement of approximately 0.700 mm is reached. From this level of displacements on, a new constant thickness reduction rate region which persists at least until maximum load is observed. This last stage accounts for more than 70% of the total thickness reduction of the center of the specimen during the test.

The actual magnitude of thickness reduction corresponding to the end of the experiment represented in Fig. 6b was verified with a micrometer. A difference less than 2.5% of the initial thickness was observed, with the total thickness reduction at this point having reached 50%.

Fig. 6b also includes the P–δ_{BOT} curve for comparison. It is interesting to see how the two curves represented resemble in their development in spite of one describing a local behavior, i.e. thickness variation of

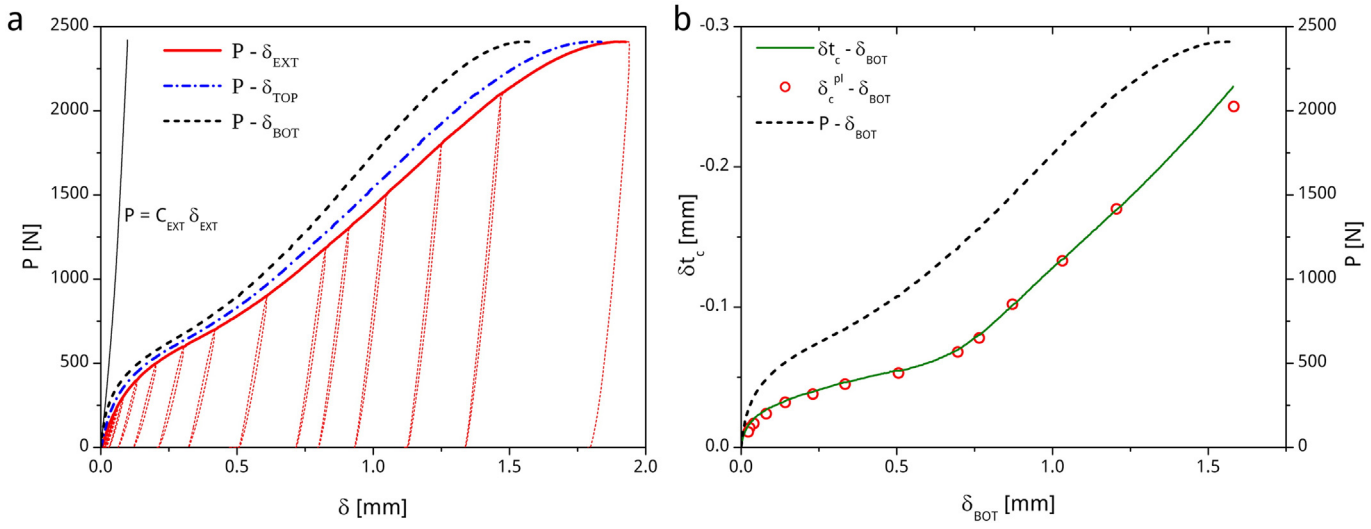

Fig. 6. Results from a SPT performed on 0.500 mm thick specimen with unloading–reloading cycles performed at progressively increasing displacements. a) P–δ curves for a corresponding to the displacements δ_{EXT}, δ_{TOP} and δ_{BOT}. b) Disk center thickness evolution along the test (see text for details).

the disk center, while the other giving the overall mechanical response of the SPT disk. This suggests that the different stages proposed for describing the mechanical response (see Introduction section) can also be identified in the curve representing the thickness evolution. A small difference however is observed in the last stage where the thickness variation with δ_{BOT} does not exhibit a region of downward curvature as it occurs in the P–δ_{BOT} curve around maximum load.

A final important issue to be discussed in the present section concerns the finite compliances of the SPT device itself and of the testing setup as a whole. On the one hand, they are responsible for the calibration corrections described in detail before but they are also an important aspect to be considered when applying SPT for fracture toughness determination, or more generally, when the study of fracture processes is intended using this technique. It is well known that more compliant testing devices result in more unstable propagation characteristics and this is even more noticeable in the case of brittle materials [32]. Thus, special care must be taken in the design of an SPT setup for studying these matters, i.e. avoiding the introduction of highly compliant components.

4.3. SPT response: comparison between numerical and experimental results

Fig. 7 shows the P–δ_{BOT} curves for the 0.500 mm thick AISI 304L disks obtained by FEM simulations employing the two extrapolations criteria for representing constitutive behavior (linear and parabolic followed by perfectly plastic). It also includes the corresponding experimental curve already presented in Fig. 6 (dashed curve to maximum load). Good agreement is observed. The simulated and experimental responses start deviating appreciably from each other only at an advanced stage of the deformation process. It is important to mention here that at such levels of deformation the disk specimen presents damage as can be appreciated in the SEM micrographs presented in Fig. 8. In effect, the observation of the bottom surface of a specimen tested until maximum load indicates, besides the presence of heavily plastically deformed grains, the occurrence of voids and microcracks. It has to be pointed out here that the discrepancies observed between the experimental and the simulated behaviors in the region near maximum load are somehow expected considering the constitutive models for material behavior assumed do not include an explicit model for damage initiation and development.

The capability of the FEM simulations of capturing other particular details of the SPT behavior beyond the overall P–δ response just described is now analyzed. For that purpose, two additional tests interrupted at loads of 700 N and 1600 N were performed. The corresponding experimental P–δ curves including unloading paths are shown in Fig. 7 where the respective interruption points are denoted by A and B. In passing, a perfect overlapping between the three experimental P–δ curves can be appreciated. This supports the statement expressed at the end of Section 2.1 about the excellent reproducibility of the SPT method here developed. Fig. 9 shows disk diametral cross section profiles for both interrupted tests. The half width images shown at the left correspond to light microscope micrographs while those shown at the right correspond to specimen profiles obtained by the FEM simulation. Again here, good agreement is observed.

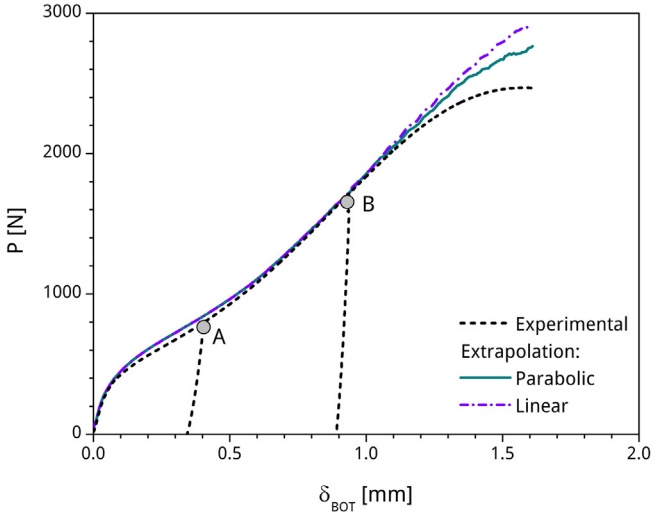

Fig. 7. Experimental and FEM simulated P–δ_{BOT} responses for 0.500 mm thick disks.

Based on the capability of reproducing both the P–δ response and the diametral cross section profile evolution along the test, it is considered that the FEM simulation tool here developed is adequate for describing the actual (experimental) SPT specimen behavior. It can then be used for the analysis of variables that are not experimentally accessible. As an example of its application, Fig. 9a and c, show the effective strain contours for the tests interrupted at 700 N and 1600 N, respectively. Similarly, Fig. 9b and d, show the corresponding von Mises stress contours. Analysis of the figures reveals strain concentration occurring in an annular region opposite to the ball contact. The zone of localized high strains moves outwards as the contact area increases. The highest strain values however are always reached close to the bottom surface. Concerning the effective stress distribution, it can be seen that the zone of high stress is coincident with the one of maximum equivalent strain. Analysis of the isovalues indicates the presence of higher stresses in a thin annular region located at the external perimeter of the contact region. From this point, gradual unloading is observed into the interior of the contact region while an abrupt stress decrease is detected moving outwards in the radial direction. This decrease in the equivalent stress in the contact region cannot be explained by the loss of contact between the ball and the specimen because this situation was verified never to occur in the simulations.

4.4. Characteristic load P_Y

In the present section, the previously validated FEM analysis tool will be applied to the study of the physical significance of different proposals considered in the literature for the evaluation of the yield stress σ_Y from the SPT mechanical response.

The basis for such evaluations is given by Eq. (1) derived from the theory of deflection of thin circular elastic plates subjected to axisymmetric loadings [33], i.e.:

$$\sigma_y = \alpha \frac{P_y}{t^2}. \tag{1}$$

Here, P_Y is a load value derived from the SPT P–δ response, t is the specimen thickness and α a calibration factor [15,27,28,34]. Different criteria have been proposed in the literature for the determination of the load P_Y. In addition, in most of the published works, the load P_Y is derived from P–δ_N or P–δ_{EXT} response curves. However, as was thoroughly discussed in a previous section, neither δ_N and δ_{EXT} represent actual displacements of the disk specimen. In the present work, actual displacements were considered and of the two options available, i.e., δ_{BOT} and δ_{TOP}, the displacement δ_{BOT} was considered for P_Y determination. Using δ_{BOT} represents an advantage compared with δ_{TOP}. In effect, the P–δ_{BOT} response exhibit a linear region in the initial states of deformation while P–δ_{TOP} includes the nonlinear behavior associated with the ceramic ball indentation on the top side of the specimen and its determination requires previous knowledge of one of the compliance calibration factors describe before.

Having adopted P–δ_{BOT} as the appropriate response to derive the load P_Y, some of the criteria reviewed in [27] were considered next for its quantitative evaluation. Mao and Takahashi [15] defined the load P_Y through the intersection point of the linear fitting lines representing stages I and II of the P–δ curve, P_Y^{MAO} in Fig. 10. This value can be considered artificial because the corresponding P–δ coordinates do not fall on

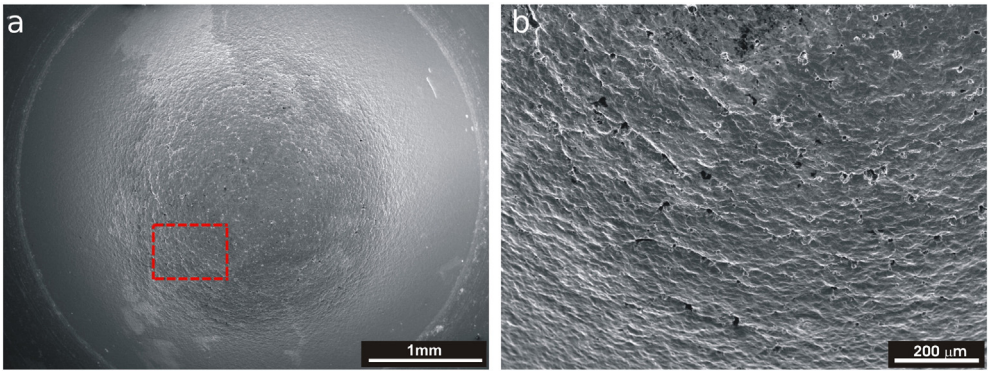

Fig. 8. SEM micrographs corresponding to disk bottom surface after testing to maximum load evidencing damage occurrence.

to the actual P–δ_{BOT} response curve and, as can be seen in the figure, the criterion can be considered to be overestimative. As indicated in Fig. 10, a more realistic value can be obtained by taking the load P_Y^{MAO*} on the P–δ_{BOT} curve corresponding to the displacement associated with P_Y^{MAO}. The other two methods that were considered here employ displacement offset values of either $t/100$ or $t/10$ for determining P_Y. They resemble the 0.2% strain offset criterion used for determining σ_Y from uniaxial tensile testing in metals not presenting a definite yield point. P–δ_{BOT} curves are particularly appropriate for application of offset type of methods due to the linearity exhibited by the curve in the initial stages of deformation. The respective P_Y values are referred to as $P_Y^{t/100}$ and $P_Y^{t/10}$ in Fig. 10. It can be seen that $P_Y^{t/100} < P_Y^{MAO*} < P_Y^{t/10}$ and that the transition between the first linear region, corresponding mainly to the elastic deflection of the disk, and the second linear region, usually assigned to plastic bending [8], exhibits a gradual development. This fact is related with the inhomogeneous deformation of the SPT specimen contributing to the indeterminacy of the derived parameters like σ_Y.

It would be now interesting to analyze the equivalent stress – stress states of the SPT specimens corresponding to the different P_Y values determined from the alternative criteria just described. This was done with the help of Fig. 11 where the FEM calculated stress – strain contours associated with the loads P_Y^{MAO*}, $P_Y^{t/100}$ and $P_Y^{t/10}$ are represented. It can be seen from Fig. 11 that, even for the lowest of the P_Y values, i.e., $P_Y^{t/100}$, in the region around the center of the disk the whole thickness of the specimen has reached or exceeded the yield limit of 652 MPa obtained from the uniaxial test (Table 1). This indicates that the spreading of the plastic deformation associated with the indentation of the ceramic ball takes place at the very early stages of the test. It can also be seen that the level of plastic strain in an annular zone close to the border of the indentation exceeded the value of the maximum uniform strain $\varepsilon_U = 0.26$ reached in the uniaxial tensile test (Fig. 4, Table 1). Fig. 11b and c describe how the effective stress and strain contours develop as the displacement is increased, firstly until reaching the load P_Y^{MAO*} (Fig. 11b) and then $P_Y^{t/10}$ (Fig. 11c). It should be noticed here that for $P_Y^{t/10}$, the whole thickness of the specimen has reached strain levels above ε_U in the annular region below the start of contact between the specimen and the ball.

It would be interesting now to assess on the volume of plastic deformed material and to analyze its evolution with the test progress. In order to do that, the volume of material with equivalent stresses levels above σ_Y (alternatively, equivalent strain above 0.002) was calculated by integration of the results calculated by FEM. The volume fraction was evaluated with respect to the volume of the central part of the disk, i.e., the region outside the clamping area between the upper and lower dies. The curve describing the evolution of plastic volume fraction with δ_{BOT} is included as the red solid line in Fig. 10. The curve presents a first region where the increase in the volume of plastic deformed

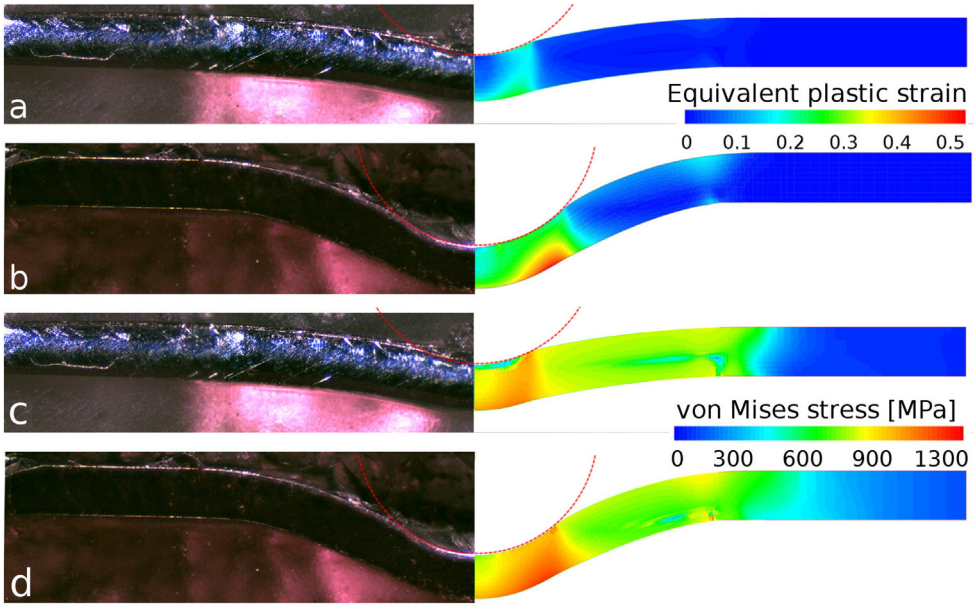

Fig. 9. Optical micrographs of experimental (left) and simulated (right) diametral cross section profiles of tests interrupted at 700 N (a and c) and 1600 N (b and d). FEM calculated effective strain and stress contours are plotted on the simulated cross section profile.

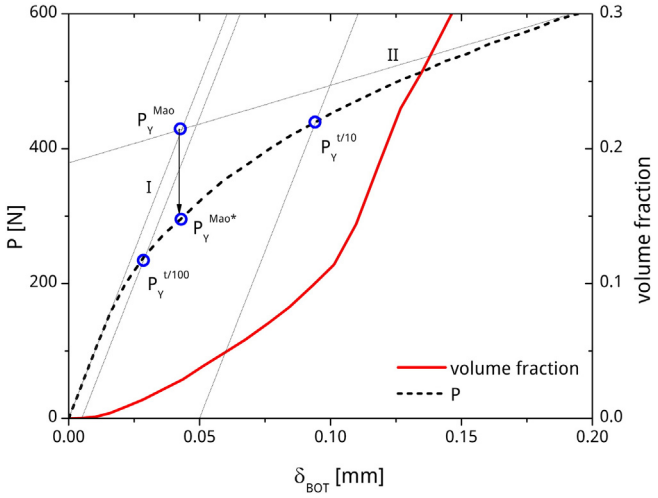

Fig. 10. Definitions of P_Y on the experimental P–δ_{BOT} plot (left vertical axis) according to the criteria of Mao (P_Y^{MAO}), modified Mao (P_Y^{MAO*}) and the offset methods $t/100$ and $t/10$ ($P_Y^{t/100}$ and $P_Y^{t/10}$). Evolution of the FEM calculated plastic deformed volume fraction for plastic strain ≥ 0.002 (right vertical axis) is included for analysis.

material is negligible. This occurs in the first 10 μm of δ_{BOT} and is coincident with the first linear region of the P–δ_{BOT}. In this range, the disk bends elastically and the plastic deformation restricts to the ball indentation zone. At a load of approximately 110 N, the volume of plastic deformed material begins augmenting with the test progress. It is only at this point when plastic deformation starts spreading through the disk specimen and from it on, the rate of increase increments gradually with δ_{BOT}. It can be seen that the three P_Y values defined before are reached inside this region. The corresponding volume fraction of plastic deformed material are 1.4% for $P_Y^{t/100}$, 2.8% for P_Y^{MAO*} and 9.3% for $P_Y^{t/10}$. At a displacement δ_{BOT} of approximately 100 μm, the rate of increase of the volume of plastic deformed material increases abruptly in coincidence with the full development of stage II in the P–δ_{BOT} curve corresponding to the plastic bending of the specimen.

The previous analysis clearly shows that the P_Y values obtained according to the different criteria discussed have an arbitrary character and correspond to different degrees of the plastic deformation of the disk specimen. Specifically, the $P_Y^{t/10}$criterion results in a P_Y value associated with a volume fraction of plastic deformed material close to 10% while for $P_Y^{t/100}$, it approaches only 2%.

These observations raise the question about the appropriateness of deriving mechanical properties, usually defined from tests performed under well-defined and simpler homogenous stress states, from much complex situations like those characterizing the SPT. In effect, using any of the criteria for P_Y determination that were discussed before would require the determination of the calibration factor α from Eq. (1). Its value will depend however on the specific material and material condition considered (heat treatment, degree of pre-deformation, etc.). These difficulties can be clearly appreciated in very recent publications [7,34] where different modifications of Eq. (1) are required to adequately describe the σ_Y–P_Y relationship. In effect, different values of factor α, and also the addition of constant terms to Eq. (1) have been proposed in [7] to derive yield properties of aluminum alloy plates subjected to different pre-straining while using different values for α have been proposed in [34] when trying to characterize SS-316L thin foils with different thickness through SPT. It is important to remark that these specific modifications are just the result of fitting procedures; the physical basis however is arguable. In this sense, the inverse method proposed by Abendroth and Kuna [35,36] using neural network training and the matching of the SPT load vs. displacement response to a curve of a database of curves proposed by [22] constitute promising alternatives.

5. Conclusions

The main conclusions that can be drawn from the combined experimental and numerical analysis performed in the previous sections are the following.

The displacement δ_{BOT} of the bottom of the specimen is the only direct measurement that does not include extra contributions neither due to the deformation of the intermediate kinematic chains nor due the ball indentation during the test. It provides an actual displacement of the SPT disk. Using any of the other displacements usually taken to represent the SPT response due to the simplicity of their determination might result in significant errors on the derived properties. The necessary corrections would require impractical experimental procedures like the calibration of the loading train compliances. Therefore, using the displacement δ_{BOT} as representative of the SPT response is highly recommendable.

Two alternative methods for determining the thickness variation of the center of the disk have been proposed. This evaluation is necessary when information about material constitutive behavior wants to be derived from SPT. Both possibilities require measuring the displacement δ_{BOT} and an additional one that can be provided by an extensometer or by the nominal displacement of the testing machine. One of the methods require the additional characterization of one compliance while the second method provides a novel, more practical, procedure

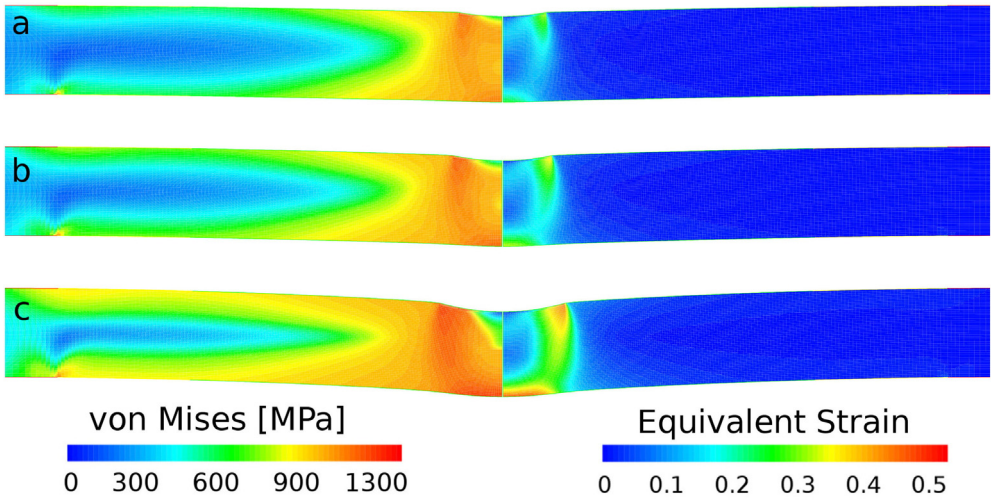

Fig. 11. Simulated cross section profiles corresponding to the loads associated with the different criteria for P_Y: a) $P_Y^{t/100}$, b) P_Y^{MAO*} and c) $P_Y^{t/10}$.

consisting in introducing repeated unloadings–reloadings loops along the test.

The results obtained from finite element simulations show that even using a constitutive model that does not include damage initiation it is possible to reproduce the SPT P–δ response curve to near maximum load. The FEM analysis tool was further validated against experimental results describing the cross section of diametral profiles and then used reliably for further analysis.

Different criteria proposed in the literature for determination of the load P_Y used for deriving yield strength from SPT have been revised in terms of P–δ_{BOT} response. The correlation between their values and the evolution of the volume fraction of plastic deformed material highlight the arbitrary character of the different definitions with the different proposal corresponding to different degrees of plastic deformation through the specimen.

A final conclusion concerning the derivation of basic mechanical properties from SPT taking into account the previous observations is that the development of the so called inverse methods that try to reconstruct the whole elastic–plastic response of the material should be favored against simpler but at the same time more arbitrary criteria for individual properties determination.

References

[1] G.E. Lucas, The development of small specimen mechanical testing techniques, J. Nucl. Mater. 117 (1983) 327–339.
[2] M.P. Manahan, A.S. Argon, K.O. Harling, The development of miniaturized disk bend test for the determination of post irradiation mechanical properties, J. Nucl. Mater. 103–104 (1981) 1545.
[3] W.R. Corwin, G.E. Lucas (Eds.), ASTM STP 888, The Use of Small Scale Specimens for Testing Irradiated Materials, ASTM, Philadelphia, 1986.
[4] W.R. Corwin, F.M. Haggag, W.L. Server (Eds.), ASTM STP 1204, Small Specimen Test Technique Applied to Nuclear Reactor Thermal Annealing and Plant Life Extension, ASTM, Philadelphia, 1993.
[5] G.E. Lucas, Review of small specimen test technique for irradiation testing, Metall. Trans. A 21A (1990) 1105–1119.
[6] I.I. Cuesta, J.M. Alegre, Influence of biaxial pre-deformation on fracture properties using pre-notched small punch specimens, Eng. Fract. Mech. 131 (2014) 1–8.
[7] I.I. Cuesta, J.M. Alegre, M. Lorenzo, Influence of strain state in mechanical behaviour of aluminium alloys using the Small Punch Test, Mater. Des. 54 (2014) 291–294.
[8] M.P. Manahan, A.E. Browning, A.S. Argon, O.K. Harling, Miniaturized disk bend test technique development and application, in: W.R. Corwin, G.E. Lucas (Eds.), ASTM STP 888, The Use of Small Scale Specimens for Testing Irradiated Materials, ASTM, Philadelphia 1986, pp. 17–49.
[9] S. Yang, X. Ling, Y. Zheng, R. Ma, Creep life analysis by an energy model of small punch creep test, Mater. Des. 91 (2016) 98–103.
[10] D. Finarelli, F. Carsughi, P. Jung, The small punch tests at FZJ, J. Nucl. Mater. 377 (2008) 65–71.
[11] K. Turba, R. Hurst, P. Hähner, Evaluation of the ductile–brittle transition temperature in the NESC-I material using small punch testing, Int. J. Press. Vessel. Pip. 111–112 (2013) 155–161.
[12] J. Ganesh Kumar, K. Laha, Small Punch Creep deformation and rupture behavior of 316L(N) stainless steel, Mater. Sci. Eng. A 641A (2015) 315–322.
[13] I. Peñuelas, I.I. Cuesta, C. Betegón, C. Rodriguez, F.J. Belzunce, Inverse determination of the elastoplastic and damage parameters on small punch tests, Fatigue Fract. Eng. M 32 (2009) 872–885.
[14] M. Lee, D.S. Sohn, N.J. Grant, O.K. Harling, Miniaturized disc bend tests of neutron irradiated path A type alloys, J. Nucl. Mater. 122–123 (1984) 146–151.
[15] X. Mao, H. Takahashi, Development of a further-miniaturized specimen of 3 mm diameter for tem disk (ϕ 3 mm) small punch tests, J. Nucl. Mater. 150 (1987) 42–52.
[16] Y. Ruan, P. Spaetig, M. Victoria, Assessment of mechanical properties of the martensitic steel EUROFER97 by means of punch tests, J. Nucl. Mater. 307–311 (2002) 236–239.
[17] D. Finarelli, M. Roedig, F. Carsughi, Small punch tests on austenitic and martensitic steels irradiated in a spallation environment with 530 MeV protons, J. Nucl. Mater. 328 (2004) 146–150.
[18] S.H. Song, R.G. Faulkner, P.E.J. Flewitt, P. Marmy, L.Q. Weng, Small punch test evaluation of neutron-irradiation-induced embrittlement of a Cr–Mo low alloy steel, Mater. Charact. 53 (2004) 35–41.
[19] S.P. Singh, S. Bhattacharya, D.K. Sehgal, Evaluation of high temperature mechanical strength of Cr–Mo grade steel through small punch test technique, Eng. Fail. Anal. 39 (2014) 207–220.
[20] M. Song, K. Guan, W. Qin, J.A. Szpunar, J. Chen, Size effect criteria on the small punch test for AISI 316L austenitic stainless steel, Mater. Sci. Eng. A 606 (2014) 346–353.
[21] G.E. Lucas, A. Okada, M. Kiritani, Parametric analysis of the disc bend test, J. Nucl. Mater. 141–143 (1986) 532–535.
[22] C. Sainte Catherine, J. Messier, C. Poussard, S. Rosinski, J. Foulds, Small punch test: EPRI-CEA finite element simulation benchmark and inverse method for the estimation of elastic plastic behavior, in: M.A. Sololov, J.D. Landes, G.E. Lucas (Eds.), Small Specimen Test Techniques: Fourth Volume, ASTM STP 1418, ASTM International, West Conshohocken, PA 2002, pp. 350–370.
[23] E.N. Campitelli, P. Spaetig, R. Bonadé, W. Hoffelner, M. Victoria, Assessment of the constitutive properties form small ball punch test: experiment and modeling, J. Nucl. Mater. 335 (2004) 366–378.
[24] S. Jitsukawa, M. Kizaki, A. Umino, K. Shiba, A. Hishinuma, Methods and devices for small specimen testing at the Japan Atomic Energy Research Institute, in: W.R. Corwin, E.M. Haggag, W.L. Server (Eds.), Small Specimen Test Techniques Applied to Nuclear Reactor Vessel Thermal Annealing and Plant Life Extension, ASTM STP 1204, ASTM, Philadelphia 1993, pp. 289–307.
[25] T.S. Byun, E.H. Lee, J.D. Hunn, K. Farrell, L.K. Mansur, A method to study deformation mechanism in ion-irradiated steels using a disk bend technique, in: M.A. Sololov, J.D. Landes, G.E. Lucas (Eds.), Small Specimen Test Techniques: Fourth Volume, ASTM STP 1418, ASTM International, West Conshohocken, PA 2002, pp. 267–282.
[26] M.B. Toloczko, R.J. Kurtz, A. Hasegawa, K. Abe, Shear punch tests performed using a new low compliance test fixture, J. Nucl. Mater. 2002 (1619–1623) 307–311.
[27] T.E. García, C. Rodríguez, F.J. Belzunce, C. Suárez, Estimation of the mechanical properties of metallic materials by means of the small punch test, J. Alloys Compd. 582 (2014) 708–717.
[28] S. Rasche, M. Kuna, Improved small punch testing and parameter identification of ductile to brittle materials, Int. J. Press. Vessel. Pip. 125 (2015) 23–34.
[29] R. Lacalle, J. García, J.A. Alvarez, F. Gutiérrez-Solana, Obtención mediante el ensayo small punch de las propiedades de tracción de materiales metálicos, Anales de Mecánica de la Fractura 26 (2009) 501–506.
[30] T.S. Byun, E.H. Lee, J.D. Hunn, K. Farrell, L.K. Mansur, Characterization of plastic deformation in a disk bend test, J. Nucl. Mater. 294 (2001) 256–266.
[31] S. Jahanmir, Friction and Wear of Ceramics, CRC Press, New York, 1993.
[32] T.L. Anderson, Fracture Mechanics: Fundamentals and Applications, 3th ed. CRC Press/Taylor and Francis Group, Boca Raton, Florida (USA), 2005.
[33] J.P. Den Hartog, Advanced Strength of Materials, McGraw-Hill Book Company, New York, 1952.
[34] S. Haroush, E. Priel, D. Moreno, A. Busiba, I. Silverman, A. Turgeman, R. Shneck, Y. Gelbstein, Evaluation of the mechanical properties of SS-316L thin foils by small punch testing and finite element analysis, Mater. Des. 83 (2015) 75–84.
[35] M. Abendroth, M. Kuna, Determination of ductile material properties by means of the small punch test and neural networks, Adv. Eng. Mater. 6–7 (2004) 536–540.
[36] M. Abendroth, M. Kuna, Determination of deformation and failure properties of ductile materials by means of the small punch test and neural networks, Comput. Mater. Sci. 28 (2003) 633–644.